This manuscript has been submitted for publication in Computers & Geosciences. Please note that, despite having undergone peer-review, the manuscript has yet to be formally accepted for publication. Subsequent versions of this manuscript may have slightly different content. If accepted, the final version of this manuscript will be available via the 'Peer-reviewed Publication DOI' link on the right-hand side of this webpage. Please feel free to contact any of the authors; we welcome feedback.

Using computer-aided image processing to estimate chemical composition of igneous rocks: A potential tool for large-scale compositional mapping

Julin Zhang*, Cin-Ty A. Lee, Michael Farner

Department of Earth, Environmental and Planetary Sciences, Rice University, Houston, TX, United States

*Corresponding author

E-mail: zhangjulin89@gmail.com

Abstract

Digital cameras, particularly on smartphones, have led to the proliferation of amateur photographers. Of interest here is the use of smartphone cameras to conduct rapid, low-cost compositional mapping of geologic bedrock, such as plutons and batholiths, in combination with chemical analyses of rocks in the laboratory. This paper discusses some of the challenges in geochemical mapping using image analysis. We discuss methods for color calibration through a series of experiments under different light intensities and conditions (spectra). All indoor and outdoor experiments show good reproducibility, but suffer from biases imparted by different light intensities, light conditions, and camera exposure times. These biases can be greatly reduced with a linear color calibration method. Over-exposed and under-exposed images, however, cannot be fully calibrated, so we discuss methods that ensure images are properly exposed. We applied our method to 59 natural granitoid samples of known chemical composition. Strong correlations between average gray levels and major element compositions were observed, indicating that very subtle variations in bulk composition can potentially be rapidly assessed using calibrated photographs of outcrops.

Keywords: mapping; image processing; color calibration; geochemistry

1. Introduction

There is a growing need for rapid, large-scale compositional mapping of outcrops and land surface as the pressures for mineral exploration and environmental assessment grow. The most accurate approach for compositional mapping is to collect samples from the field and analyse them in the laboratory through various geo-analytical methods (X-ray fluorescence, inductively coupled plasma mass spectrometry, etc.), but these approaches are too expensive and too slow to fully support rapid, large-scale compositional mapping (Potts, 2012). There is thus a need to explore other methods that may be less precise but compensate for this deficiency by allowing for the accumulation of large datasets. The best trained geologists serve as walking image processers and analyzers as they are trained to identify rocks and interpret their origins from rock textures and colors based solely on the unaided eye and years of experience. Human eyes and brains are not the same, so considerable observer variability and bias is introduced when more than one geologist is conducting a lithological survey. Computer-aided processing of rock textures has thus become an important part of quantifying such quantities as grain size, shape and spatial distribution in igneous and metamorphic petrology (Åkesson et al., 2003; Cashman and Ferry, 1988; Cashman and Marsh, 1988; Heilbronner, 2000; Jerram et al., 2003; Kemeny et al., 1993).

In this paper, we explore the use of color in quantifying the composition of igneous rocks. Because color can correlate with mineralogy, it might be expected to correlate with composition for a certain range of geologic materials. There are, however, many challenges in using color quantitatively because many variables control color and its perception (Stevens et al., 2007). For example, alteration can easily modify the surface color of mineral grains. In addition, apparent color varies

depending on the spectrum of light, which can change throughout the day or under different lighting conditions (Foster, 2011; Romero et al., 2003). There is thus a need for robust color calibration, particularly if color is being assessed outdoors when conditions change continually. In the soil science community, eye-based side-by-side comparison with the Munsell color chart has been widely used to quantify soil color in the field (Color, 1998; Pendleton and Nickerson, 1951; Rossel et al., 2006). Similar computer-based calibration against color guides (Joshi and Jensen, 2004; Pascale, 2006) has been applied to problems in food science, biosciences, agriculture and planetary exploration (Allender et al., 2018; Costa et al., 2010; Fischer, 2019; Wu and Sun, 2013).

Here, we develop a method for quantifying color from images taken from simple hand-held digital cameras or phone cameras, opening an opportunity for large-scale, high resolution mapping using citizen science. We note that the development of plant and animal identification algorithms in mobile phone apps has decreased the barriers for citizens to report observations, resulting in the largest and most comprehensive biodiversity survey of the planet to date, a feat that could never have been accomplished by all living scientists combined (Sullivan et al., 2014; Van Horn et al., 2018). Our long-term goal is to use color and texture-based image analysis to map out compositional variations of a pluton on the scale of meters or less. Our long term goals are to be able to use such compositional maps to better understand the dynamics of magmatic systems. This paper is a small step towards that goal. It is the hope that subtle variations in composition can be detected by quantifying subtle variations in color.

2. Material and methods

2.1. Samples

Image analyses were conducted on felsic granitoids from the Bernasconi Hills pluton, northern Peninsular Ranges Batholith in California, USA (Farner et al., 2017). The samples consist primarily of quartz and plagioclase with small amounts of hornblende and biotite. Felsic or silicic minerals, such as quartz and plagioclase, appear as transparent or white, whereas mafic minerals like hornblende and biotite are dark brown to black. Our goal was to quantify the "mafic index", that is, the bulk gray level and relative proportions of dark minerals using image analysis, and in particular, to explore the challenges of quantifying mafic index under variable lighting conditions.

2.2. Experimental setup

We first conducted a series of indoor experiments under controlled light conditions to gain a sense of how ambient light affects perceived color. In all experiments, we used an iPhone 7 Plus digital camera with an aperture of f/1.8. For indoor lighting, we used two TaoTronics™ LED table lamps (12 W and 410 lumens). These LED table lamps have 5 lighting conditions (cold white - CW, white - W, natural - N, yellow -Y and warm yellow - WY) and 7 intensity levels where level 1 refers to the lowest intensity and level 7 for highest intensity. The two LED lamps were placed 26 cm over the sample and with a separation distance between the two lamps of 23 cm to minimize shadows (Fig. 1(a)). The camera was placed slightly higher than the lamps to avoid generating shadows (Fig. 1(a)). A phone holder and camera shutter remote control were used to avoid vibrations.

In order to calibrate color, we placed a X-Rite ColorChecker Passport™, which has 24 pure color patches with known sRGB values, adjacent to the rock sample for all photographs (Fig. 1(b)). Instead of using the default camera application in the iPhone 7 Plus, which stores images in the form of JPEGs, photographs were taken using an App called Camera+™. Camera+™ stores images in DNG format, which is a raw file format that does not normalize the spectral histogram of an image. Camera+™ also allows the option to manually change camera settings, such as exposure time and ISO, etc. However, for indoor experiments, we used auto mode, which allows the program to automatically choose the proper exposure time and ISO.

Image experiments were also performed outdoors under natural daylight conditions. Due to the high intensity of daylight and the ease to which iPhone cameras become saturated, pictures taken with an iPhone under bright daylight are usually overexposed, making it difficult if not impossible to calibrate an overexposed image. To solve this problem, we attached a PolarPro™ Iris neural density filter (ND filter) in front of the camera lens. We used the ND8 filter, which reduces the amount of incident light by a factor of 8 but does not change the spectrum of the incident light. Unlike the auto mode choice for indoor experiments, we manually set the exposure time and ISO for outdoor experiments and explored the effect of camera settings on the performance of the calibration.

2.3. Calibration method

Because the colors of minerals in our rock samples are primarily black and white, we studied the gray level histogram of the images instead of three separated RGB histograms. The algorithm of converting RGB tristimulus values of a pixel in the sRGB color space to one gray level value used in this paper follows the ITU-R Recommendation BT.601(BT, n.d.):

$$Gray = Red * 0.299 + Green * \ 0.587 + Blue * 0.114 \quad (1)$$

Luminosity calibration is usually required before color calibration to compensate for spatially heterogeneous transmission of light across the camera lens area (Hong et al., 2001; Losey, 2003). We used a white calibration board on the X-Rite ColorChecker Passport™ to check for spatial homogeneity of luminosity distribution by placing the white board in exactly the same positions where the sample and the color checker would sit. The same camera settings were adopted for all photographs (exposure time of 1/120 and ISO of 25). Our results show that the gray level histograms of the two areas (sample and color checker) were very similar, with mean grayscale values within 2% (Fig. 2(a,b)). There was thus no need to perform any luminosity calibrations before color calibrations. In the field, so long as the light source is diffuse on the length scale of the sample, luminosity corrections are not needed.

Color was calibrated with the X-Rite ColorChecker Passport™, which offers 24 color patches with known sRGB values. RGB measurements of each of the 24 color patches were mapped to the 'real' RGB tristimulus values to develop a calibration model for each photograph. A linear model shown below was assumed:

$$Red_{calib} = \alpha_0 + \alpha_1 * Red + \alpha_2 * Green + \alpha_3 * Blue$$

$$Green_{calib} = \beta_0 + \beta_1 * Red + \beta_2 * Green + \beta_3 * Blue$$

$$Blue_{calib} = \gamma_0 + \gamma_1 * Red + \gamma_2 * Green + \gamma_3 * Blue \quad (2)$$

where Red_{calib}, $Green_{calib}$ and $Blue_{calib}$ refer to the red, green and blue values of a pixel in the rock image after calibration, Red, $Green$ and $Blue$ represent the actual RGB values of the standard, and α, β and γ are the parameters of the model. These parameters are determined by least squares fitting of the data to the above model.

2.4. Feature extraction from histograms

The gray level histogram of the rock image is assumed to be a mixture of two signals, each of which represents the signal of a dark or light mineral group. These two signals can be segmented by Otsu thresholding algorithm (Otsu, 1979). The dark and light mineral proportions were then estimated based on the binarization result. In addition, the average gray level intensity of histograms, which evaluate the overall gray level intensity of the rock image, also was considered in this study. All the programs in this study were coded in Python 3.6 (code can be accessed via https://github.com/Zhangjulin/Color_calibration/blob/master/Color_calibration.py).

3. Results

3.1. Reproducibility of indoor and outdoor experiments

In order to evaluate internal reproducibility, images of a same rock sample along with the color checker (Fig. 1(b)) were taken 10 times under the same light condition. We checked the consistency of gray level histograms among these 10 images before and after color calibration. The reproducibility experiments were done both indoor and outdoor. For the indoor reproducibility experiments, two LED lamps were set to white (W) light condition and intensity level of 5. Auto mode on the iPhone was used, resulting in an exposure time of 1/300 and ISO of 25. For the outdoor reproducibility experiments under daylight, we attached a ND8 filter to the iPhone camera to avoid overexposure and we manually set the exposure time to 1/750 and ISO to 25.

The results show that both indoor and outdoor histograms have good internal consistency before and after color calibration (Fig. 3). We note that there is a small spike at gray level intensity of 0 in the outdoor non-calibrated histograms (Fig. 3(c)), indicating a slight underexposure. In any case, histograms are bimodal with the left

peak representing the dark mineral mode and the right peak representing the light mineral mode. These two modes overlap between gray level intensity 60 to 130.

Average gray level intensities and mineral proportions were later determined from calibrated histograms. We also evaluated reproducibility of these two indices. The results show that the mean value of dark mineral proportion for indoor experiments is 0.365 with a relative two standard deviation (2RSD) of 1.54% while the mean and 2RSD for outdoor experiments are 0.354 and 0.680% (detailed data can be found in the supplemental materials). The mean and 2RSD of dark mineral proportion between indoor and outdoor experiments were similar. The average gray level for indoor experiments is 125.2 (2RSD = 0.12%) and 117.2 (2RSD = 0.22%) for outdoor experiments.

3.2. Indoor experiments

We accumulated 35 images of a same granitoid sample (Fig. 1(b)) indoors with different LED light conditions or intensities. The gray level histograms of these 35 images after color calibration show more internal consistency than before color calibration (Fig. 4). The discrepancy of uncalibrated histograms comes from the difference in LED light conditions and intensities.

We first checked the RGB measurements of the color checker to see how light intensity biases color. Fig. 5 shows measured versus actual color for the color checker under CW, W, N, Y and WY light conditions with intensity levels of 1, 5 and 7. Every data point in Fig. 5 represents red (green or blue) measurements corresponding to the 24 calibration standards. Deviations from the 1:1 line indicate measurement bias. All experiments show some level of bias. For Y and WY light conditions, the degree of bias appears to be independent of intensity level (Fig. 5(j-o)). This is because the iPhone auto exposure program adequately changes exposure time and ISO to

compensate for different light intensity. Bias remains constant for CW, W, and N light conditions when intensity increases from level 1 to level 5 (Fig. 5(a,b,d,e,g,h)), but when intensity increases to level 7, there is an increase in the negative deviation of measured values compared to standard values (Fig. 5(c,f,i)).

Of particular interest is how the degree of bias varies between different light conditions, which would indicate that the spectrum of light influences color perception. For an intensity level of 5 (Fig. 5(b,e,h,k,n)), measurements under CW, W and N mostly fall close to the 1:1 line (Fig. 5(b,e,h)), with the exception of measurements lower than 100, which fall below the 1:1 line. We also note that the blue data are systematically higher than the green and red data. When Y light is used, some blue data go to zero, indicating underexposure (Fig. 5(k)). Unlike CW, W and N light conditions, the red data under Y light conditions are systematically higher than the green and blue data. For WY light, red, green and blue data all show significant bias from the standard (Fig. 5(n)) although the data parallel the 1:1 line.

The color biases observed for the different light conditions are undoubtedly due to differences in the spectrum of the 5 light conditions. CW and W light have more short wavelength light (blue) but less long wavelength light (red), so the reflected light of the color checker will have more blue than red light (Fig. 5(b,e)). In contrast, Y and WY light have more long wavelength light than short wavelength light, and as a consequence, the reflected light has more red than blue light (Fig. 5(k,n)).

The above experiments were also used to explore the effects of light intensity and light condition (spectrum) on gray level histograms (Fig. 6-7). Uncalibrated histograms regardless of light condition are consistent between light intensities of 1-5 (Fig. 6(a,c-f)), but shift darker at intensity level of 6 and 7 for CW, W and N light

conditions (Fig. 6(a,c,d)). However, after calibration, histograms converge and are consistent across all light intensities (Fig. 6(b)). The calibrated histograms become slightly compressed compared to the uncalibrated histograms (Fig. 6(a,b)).

The effects of light condition on gray level histograms were also explored. Fig. 7(a,c,e) show the comparisons of uncalibrated gray level histograms for different light conditions under the same light intensity level (1, 4 and 7). Varying light condition caused the centroid of dark and light minerals to migrate. In particular, the light mineral mode in WY light becomes compressed and shifts darker compared to other light conditions, although this effect diminishes when light intensity increases to 7 (Fig. 7(e)). After calibration, histograms in WY light converge to that of other light conditions (Fig. 7(b,d,f)).

Average gray level and mineral proportions were estimated from both uncalibrated and calibrated histograms. The mean value of average gray level of uncalibrated histograms is 115.0 (2RSD = 6.2%) and that of calibrated histograms is 125.3 (2RSD = 0.78%). The mean value of calibrated results is ~9% larger than for the uncalibrated results, and the variance of calibrated results is much smaller. The mean value of the dark mineral proportion estimated from uncalibrated histograms is 0.359 (2RSD = 2.68%), and 0.360 (2RSD = 2.80%) for calibrated histograms. The mineral proportion estimated from uncalibrated and calibrated histograms are similar. While mean grayscale and mineral proportion values are similar for different lighting conditions, there is more variation in the magnitude of the 2RSDs across light conditions (Table 1). CW light displays the largest variability whereas WY light displays the smallest variability, with 2RSD decreasing as the softness of light increases.

3.3. Outdoor experiments under uncontrolled daylight

In order to study the influence of dynamic daylight in gray level histograms, we conducted 20 series of outdoor experiments at different times of the day (from morning to afternoon) and on days with different lighting conditions (sunny and cloudy days).

Here, we present the results of one representative outdoor experiment performed on a sunny afternoon. We first explored auto mode (exposure time of ~1/3500 and ISO of 20). Nearly all RGB measurements of the color checker deviate positively from the standard values (Fig. 8(a)). Some RGB measurements even approach the saturation limit (255), which indicates overexposure. The uncalibrated histogram under auto mode shifts much lighter compared to indoor uncalibrated histograms as exemplified in Fig. 8(b) for N light condition and intensity level of 4. A linear color calibration was found to fix the shift but there remains obvious discrepancy between the histogram shape, especially towards the dark mineral mode (Fig. 8(c)).

To improve on this, we attached a ND8 filter to the iPhone 7 Plus, which reduces the amount of light transmitted to the camera. Images were taken with a series of different exposure times (1/500, 1/750, 1/1000 and 1/1500) with ISO manually fixed to 25 to be consistent with the indoor experiments. The exposure time of 1/500 combined with a ND8 filter still results in overexposure and does not improve results (Fig. 8(d-f)). When the exposure time decreases to 1/750 and 1/1000, the discrepancy between measurements and standards in the color checker are reduced, and both the uncalibrated and calibrated histograms match better with reference histograms (Fig. 8(g-l)). However, when exposure time decreases to 1/1500, all the RGB measurements fall below the corresponding standards due to underexposure (Fig. 8(m)). This underexposure drives the uncalibrated histogram to shift darker (Fig. 8(n))

and worsens the calibrated histogram (Fig. 8(o)). These results show that a too small or too large exposure time will distort the histogram even after calibration. Therefore, an optimal exposure time window is necessary, and for this outdoor experiment, exposure time of 1/750-1/1000 is favored.

The results of other 19 outdoor experiments show that the optimal exposure time varies under different daylight conditions (see supplemental data). Average gray levels and dark mineral proportions of there 20 outdoor experiments were determined from calibrated histograms that are properly exposed. The mean value of average gray levels for these 20 experiments is 115.5 (2RSD = 4.3%, Table 2). The outdoor mean value is ~8% lower than the indoor result (125.3, 2RSD = 0.78%) and has a larger 2RSD. The mean value of dark mineral proportions is 0.365 (2RSD = 8.07%), which is close to the indoor result (0.360, 2RSD = 2.80%) but has a larger 2RSD. Without the assistance of a ND filter, both the average gray level (115.9, 2RSD = 6.0%) and mineral proportion estimates (0.339, 2RSD = 18.6%) exhibit much larger variation (Table 2).

4. Discussion

4.1. Prospects and pitfalls of indoor imaging

The reproducibility tests show that an iPhone 7 Plus, combined with Camera+ APP, is able to obtain consistent gray level histograms under the same light condition (Fig. 3(a,c)). The linear color calibration method maintains this consistency even though histogram shapes are changed (Fig. 3(b,d)). Limited variation of average gray level and dark mineral proportions estimated from calibrated histograms indicate that our method is robust.

Indoor experiments show that varying light conditions impacts color information (Fig. 5). Differences in light conditions or intensity can lead to inconsistency of gray level histograms on the same rock sample (Fig. 6(a,c-f) and Fig. 7(a,c,e)). However, we showed that consistency can be improved significantly with a linear calibration (Fig. 6(b) and Fig. 7(b,d,f)), supporting the validity of our method to calibrate histograms under indoor conditions.

4.2. Prospects and pitfalls of outdoor imaging

Outdoor experiment results show that auto mode is very likely to overexpose images (Fig. 8(a,b)). We also show that a linear calibration cannot perfectly calibrate the histograms (Fig. 8(c)). Therefore, for field geological mapping, it is wise to use manual mode with a ND filter and set proper exposure time appropriate to the daylight condition (Fig. 8(d-o)). However, it is difficult to determine the optimal exposure time if an indoor reference is not known, which would likely be the case for the casual citizen scientist. One way to solve this problem is to check the measurement-standard diagram of the color checker to see whether all the data lies around the 1:1 line, but this approach may be too qualitative.

Here, we explore a more quantitative method to determine the optimal exposure time window under arbitrary daylight conditions without knowledge of an indoor reference. Based on the consistency between indoor and outdoor histograms, we categorized all 90 images from 20 outdoor experiments into three groups: proper exposed images, underexposed images, and overexposed images. These three groups can be well classified by the red channel measurement of the orange patch (‘I’ in Fig. 9(a)) and blue patch (‘II’ in Fig. 9(a)) of the color checker since the red channels of these two colors are sensitive to the light intensity change (Fig. 9(b)). The blue, red and black data symbols in Fig. 9(b) represent the overexposed, proper exposed and

underexposed data, respectively. Under proper exposure, data fall in a window bounded by the overexposed and underexposed data (Fig. 9(b)): 225-240 for the orange patch and 10-30 for the blue patch. For other brand color checkers, the optimal window for those two patches may be different and needs to be studied.

4.3. Estimating dark and light mineral proportions

Average gray level and dark mineral proportion were determined from the histograms. Overall, these two indexes of indoor experiments vary much smaller than outdoor experiments (Table 2). This may due to the uncontrolled property of daylight. Indoor experiment results show that the average gray level of calibrated histograms has much smaller variation (2RSD = 0.78%) than uncalibrated histograms (2RSD = 6.2%). This means that calibration can greatly improve the consistency of average gray level under different light conditions. The dark mineral proportion results between calibrated and uncalibrated histograms are similar. This is because within the variability of indoor light conditions, calibration does not significantly change the shapes of the histograms which determine the Otsu thresholding results. In contrast, for the outdoor experiments without ND filter, calibration significantly changes the shapes of histograms (Fig. 8(c)). Therefore, the dark mineral proportion results (0.339, 2RSD = 18.6%) are not consistent well with the indoor experiments (0.360, 2RSD = 2.80%, Table 2). The much better result of proper exposed outdoor experiments with a ND filter (0.365, 2RSD = 8.07%, Table 2) supports the necessarity of ND filter under daylight condition.

4.4. Application to petrology

The calibration method proposed in this paper can provide precise and consistent histograms, which store valuable color information, of rock samples under

different light conditions. Some features, such as average gray level, of the histograms may correlate with chemical components of rocks considering the association between color information and mineralogy. To test this hypothesis, we did indoor experiments on 59 rock samples for which bulk chemical compositions were analyzed by XRF. These rocks are from the Bernasconi Hills pluton in the northern Peninsular Ranges Batholith in California, USA(Farner et al., 2017). Thirty-five of these samples are felsic granitoids and the remaining are mafic enclaves. Only the fresh faces of rock samples were used here since weathering can cause discoloration of mineral surfaces. We followed our indoor protocols outlined above. Rock samples were placed under two LED lamps along with a color checker for color calibration. All the 59 experiments were carried out under N light condition and light intensity level of 4.

The results show that the average gray levels of calibrated histograms correlate well with some chemical components (Fig. 10). Gray scale correlates negatively with FeO, MnO and MgO, and positively with SiO_2, which we attribute to the fact that the most abundant dark mineral in these samples is hornblende, which is rich in Fe, Mn and Mg. For FeO and MnO, the R^2 of correlations can reach 0.9 (Fig. 10(a,b)), and for MgO and SiO_2 are above 0.85 (Fig. 10(c,d)). Given the fact that outdoor 2RSD result of average gray level is ~4.3% (Table 2), these correlations from indoor experiments imply that our method may also work for outdoor compositional mapping. In this paper, we only explored the correlation between average gray level and chemical composition. Some mining industry studies show that the correlation can be improved further if more color features or even textural features are incorporated (Bonifazi et al., 2001; Haavisto et al., 2006; Hargrave and Hall, 1997; Hargrave et al., 1996; Oestreich et al., 1995). Therefore, a more generalizable model

can be developed as more features and data are accumulated, serving potentially as a powerful tool to predict the chemical compositions of rock by image analysis.

There are of course some limitations in our method. In this paper, we focus on the gray level histograms because our rock samples only have dark and light minerals. For rocks containing more 'colorful' minerals, it will be better to study the three RGB histograms separately or even to consider the HSI color space. However, this paper is a step towards this direction of full color image analysis. In the future, we hope to explore other features, such as peak amplitude, peak width, etc.

5. Conclusions

In this paper, we proposed a simple but detailed method for imaging and color calibration of rocks using a digital camera on an iPhone 7 Plus. This simple color calibration method, assisted with a color checker as standard, can greatly improve the consistency of gray level histograms of the rock sample under different light conditions. We also showed that average gray levels of calibrated histograms strongly correlate with some chemical contents of 59 plutonic rocks, indicating that our method has potential for being an efficient tool for compositional mapping at large scale.

Acknowledgements

We thank Luca Giancardo for his generous advice on image processing. We thank Ming Tang and Wenrong Cao for discussions. This work was supported by the U.S. NSF via EAR- 1753599.

Disclosure statement

No potential conflict of interest was reported by the authors.

References

Allender, E.J., Stabbins, R.B., Gunn, M.D., Cousins, C.R., Coates, A.J., 2018. The ExoMars Spectral Tool (ExoSpec): an image analysis tool for ExoMars 2020 PanCam imagery, in:. Presented at the Image and Signal Processing for Remote Sensing XXIV, International Society for Optics and Photonics, p. 107890I.

Åkesson, U., Stigh, J., Lindqvist, J.E., Göransson, M., 2003. The influence of foliation on the fragility of granitic rocks, image analysis and quantitative microscopy. Engineering Geology 275–288.

Bonifazi, G., Serranti, S., Volpe, F., Zuco, R., 2001. Characterisation of flotation froth colour and structure by machine vision. Computers & Geosciences 27, 1111–1117.

BT, R.I.-R., n.d. Studio encoding parameters of digital television for standard 4: 3 and wide-screen 16: 9 aspect ratios.

Cashman, K.V., Ferry, J.M., 1988. Crystal size distribution (CSD) in rocks and the kinetics and dynamics of crystallization. Contributions to Mineralogy and Petrology 99, 401–415.

Cashman, K.V., Marsh, B.D., 1988. Crystal size distribution (CSD) in rocks and the kinetics and dynamics of crystallization II: Makaopuhi lava lake. Contributions to Mineralogy and Petrology 99, 292–305.

Color, M., 1998. Munsell soil color charts. Munsell Color.

Costa, C., Pallottino, F., Angelini, C., Proietti, M., Capoccioni, F., Aguzzi, J., Antonucci, F., Menessati, P., 2010. Colour calibration for quantitative biological analysis: A novel automated multivariate approach. Instrumentation viewpoint 70–71.

Farner, M.J., Lee, C.-T.A., Mikus, M.L., 2017. Geochemical signals of mafic-felsic mixing: Case study of enclave swarms in the Bernasconi Hills pluton, California. GSA Bulletin 130, 649–660. doi:10.1130/B31760.1

Fischer, T., 2019. PCA-based supervised identification of biological soil crusts in multispectral images. MethodsX 6, 764–772.

Foster, D.H., 2011. Color constancy. Vision research 51, 674–700.

Haavisto, O., Kaartinen, J., Hyotyniemi, H., 2006. Optical spectrum based estimation of grades in mineral flotation, in:. Presented at the 2006 IEEE International Conference on Industrial Technology, IEEE, pp. 2529–2534.

Hargrave, J.M., Hall, S.T., 1997. Diagnosis of concentrate grade and mass flowrate in tin flotation from colour and surface texture analysis. Minerals Engineering 10, 613–621.

Hargrave, J.M., Miles, N.J., Hall, S.T., 1996. The use of grey level measurement in predicting coal flotation performance. Minerals Engineering 9, 667–674.

Heilbronner, R., 2000. Automatic grain boundary detection and grain size analysis using polarization micrographs or orientation images. Journal of Structural Geology 22, 969–981.

Hong, G., Luo, M.R., Rhodes, P.A., 2001. A study of digital camera colorimetric characterization based on polynomial modeling. Color Research & Application: Endorsed by Inter-Society Color Council, The Colour Group (Great Britain), Canadian Society for Color, Color Science Association of Japan, Dutch Society for the Study of Color, The Swedish Colour Centre Foundation, Colour Society of Australia, Centre Français de la Couleur 26, 76–84.

Jerram, D.A., Cheadle, M.J., Philpotts, A.R., 2003. Quantifying the building blocks of igneous rocks: are clustered crystal frameworks the foundation? Journal of Petrology 44, 2033–2051.

Joshi, N., Jensen, H.W., 2004. Color calibration for arrays of inexpensive image sensors. Master's with Distinction in Research Report, Stanford University, Department of Computer Science 30.

Kemeny, J.M., Devgan, A., Hagaman, R.M., Wu, X., 1993. Analysis of rock fragmentation using digital image processing. Journal of Geotechnical Engineering 119, 1144–1160.

Losey, G.S., Jr, 2003. Crypsis and communication functions of UV-visible coloration in two coral reef damselfish, Dascyllus aruanus and D. reticulatus. Animal Behaviour 66, 299–307.

Oestreich, J.M., Tolley, W.K., Rice, D.A., 1995. The development of a color sensor system to measure mineral compositions. Minerals Engineering 8, 31–39.

Otsu, N., 1979. A threshold selection method from gray-level histograms. IEEE transactions on systems, man, and cybernetics 9, 62–66.

Pascale, D., 2006. RGB coordinates of the Macbeth ColorChecker. The BabelColor Company 6.

Pendleton, R.L., Nickerson, D., 1951. Soil colors and special Munsell soil color charts. Soil Science 71, 35–44.

Potts, P.J., 2012. A handbook of silicate rock analysis. Springer Science & Business Media.

Romero, J., Hernández Andrés, J., Nieves, J.L., García, J.A., 2003. Color coordinates of objects with daylight changes. Color Research & Application: Endorsed by Inter-Society Color Council, The Colour Group (Great Britain), Canadian Society for Color, Color Science Association of Japan, Dutch Society for the Study of Color, The Swedish Colour Centre Foundation, Colour Society of Australia, Centre Français de la Couleur 28, 25–35.

Rossel, R.V., Minasny, B., Roudier, P., McBratney, AB, 2006. Colour space models for soil science. Geoderma 133, 320–337.

Stevens, M., Párraga, C.A., Cuthill, I.C., Partridge, J.C., Troscianko, T.S., 2007. Using digital photography to study animal coloration. Biological Journal of the Linnean society 90, 211–237.

Sullivan, B.L., Aycrigg, J.L., Barry, J.H., Bonney, R.E., Bruns, N., Cooper, C.B., Damoulas, T., Dhondt, A.A., Dietterich, T., Farnsworth, A., 2014. The eBird enterprise: an integrated approach to development and application of citizen science. Biological Conservation 169, 31–40.

Van Horn, G., Mac Aodha, O., Song, Y., Cui, Y., Sun, C., Shepard, A., Adam, H., Perona, P., Belongie, S., 2018. The inaturalist species classification and detection dataset, in:. Presented at the Proceedings of the IEEE conference on computer vision and pattern recognition, pp. 8769–8778.

Wu, D., Sun, D.-W., 2013. Colour measurements by computer vision for food quality control–A review. Trends in Food Science & Technology 29, 5–20.

Tables

Table 1. Average gray levels and dark mineral proportions estimated from calibrated histograms under different light conditions

Light condition	*Average gray level*		*Dark mineral proportion*	
	Mean	*2RSD*	*Mean*	*2RSD*
Cold white (CW)	125.2	0.59%	0.357	3.95%
White (W)	125.4	0.42%	0.358	1.81%
Natural light (N)	125.6	0.27%	0.357	1.29%
Yellow (Y)	125.7	0.16%	0.359	1.75%
Warm yellow (WY)	124.5	0.18%	0.366	0.491%
All	125.3	0.78%	0.360	2.80%

Table 2. Average gray levels and dark mineral proportions estimated from calibrated histograms indoors and outdoors

Light condition	*ND filter*	*Average gray level*		*Dark mineral proportion*	
		Mean	*2RSD*	*Mean*	*2RSD*
Indoor	No	125.3	0.78%	0.360	2.80%
Outdoor	Yes	115.5	4.3%	0.365	8.07%
Outdoor	No	115.9	6.0%	0.339	18.6%

Figure legends

Figure 1. Indoor experiment environment and materials used in this project. (a) Two LED lamps were placed in parallel over the sample. An iPhone was placed above the lamps. (b) A granitoid sample, along with a color checker, was placed under the lamps.

Figure 2. Results of luminosity experiments. (a) Comparison of two gray level histograms of the same white board placed at the positions where the sample (orange histogram) and the color checker (blue histogram) should sit. (b) Zoomed in view of (a). Gray level mean for sample and color checker locations are ~185 and ~190, respectively.

Figure 3. Results of reproducibility experiments. (a) Indoor result before calibration, (b) indoor result after calibration, (c) outdoor result before calibration and (d) outdoor result after calibration. Each panel shows the results of 10 independent experiments.

Figure 4. Gray level histograms of the same granitoid sample under different indoor LED light conditions and intensities. (a) Histograms before color calibration and (b) histograms after color calibration.

Figure 5. Measurement of color-checker standards under different indoor light conditions and intensities. X-axis represents standard values and Y-axis represents measured gray level. Color (red, green and blue) of each data point refers to the RGB tristimulus value of a particular color patch on the color checker. (a)-(c) CW light ,

(d)-(f) W light, (g)-(i) N light (j)-(l) Y light, and (m)-(o) WY light. Light intensity was fixed to level 1, 5 and 7 (columns).

Figure 6. Gray level histograms of granitoid sample under constant indoor light conditions but different intensities. (a) Uncalibrated and (b) calibrated histograms under CW light condition with different light intensity levels. Uncalibrated histograms under (c) W , (d) N , (e) Y , and (f) WY light with different light intensity levels.

Figure 7. Gray level histograms of the granitoid sample under constant indoor light intensity but different light conditions. (a) Uncalibrated and (b) calibrated histograms under different light conditions with light intensity fixed to level 1. (c) Uncalibrated and (d) calibrated histograms under different light conditions with light intensity fixed to level 4. (e) Uncalibrated and (f) calibrated histograms under different light conditions with light intensity fixed to level 7.

Figure 8. Outdoor color calibration results with different exposure times. (a) Comparison of measured gray scale to standard values of the color checker, (b) uncalibrated and (c) calibrated histograms of the granitoid sample when using auto exposure. The results when manually setting the exposure time to (d)-(f) 1/500, (g)-(i) 1/750, (j)-(l) 1/1000 and (m)-(o) 1/1500 seconds.

Figure 9. A quantitative method to determine the optimal exposure time window under arbitrary daylight conditions. (a) Orange and blue patches in the color checker were analyzed. (b) Red channel measurements of orange and blue patch for

20 outdoor experiments with different exposure times. The blue, red and black data points represent overexposed, properly exposed and underexposed data, respectively.

Figure 10. Correlations between average gray level of calibrated histograms and major element contents from 59 rock samples. Gray scale correlates negatively with whole-rock (a) FeO, (b) MnO and (c) MgO, and positively with (d) SiO_2 (wt. %).

Fig.1

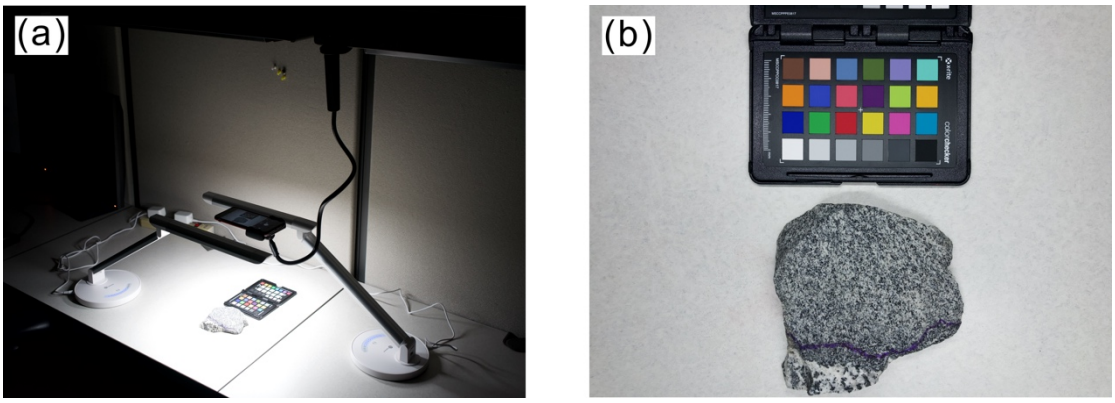

Fig.2

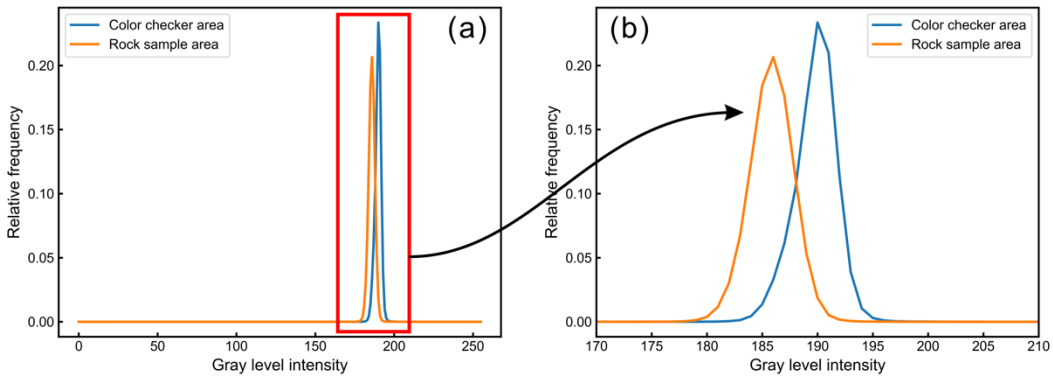
(a)
(b)
Color checker area
Rock sample area
Relative frequency
Gray level intensity
0.00
0.05
0.10
0.15
0.20
0
50
100
150
200
250
170
175
180
185
190
195
200
205
210

Fig.3

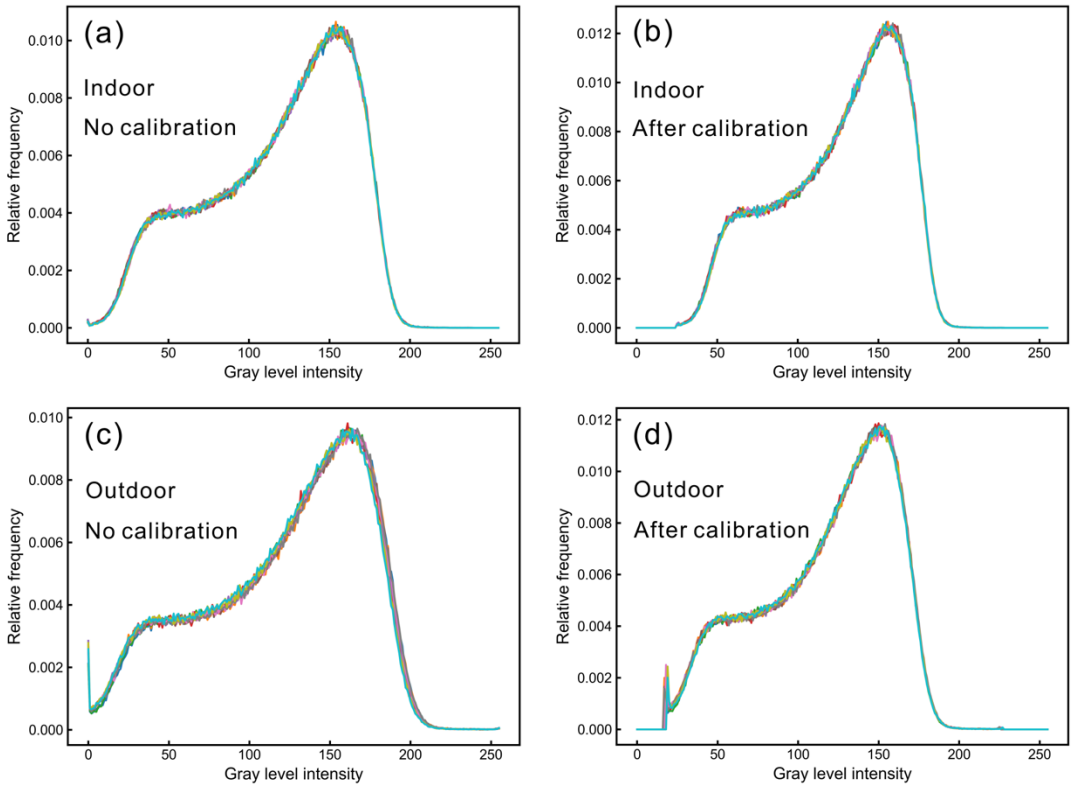
(a)
Indoor
No calibration
(b)
Indoor
After calibration
(c)
Outdoor
No calibration
(d)
Outdoor
After calibration
Relative frequency
Gray level intensity

Fig.4

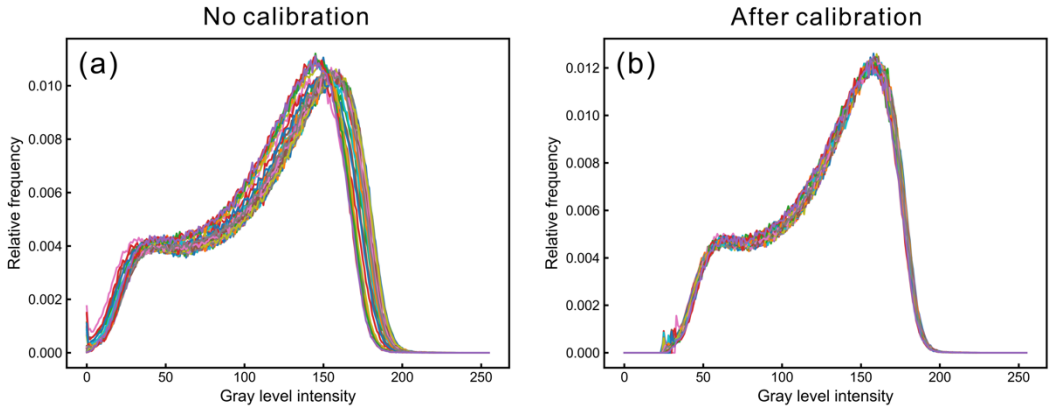
No calibration
(a)
Relative frequency
0.010
0.008
0.006
0.004
0.002
0.000
0
50
100
150
200
250
Gray level intensity
After calibration
(b)
Relative frequency
0.012
0.010
0.008
0.006
0.004
0.002
0.000
0
50
100
150
200
250
Gray level intensity

Fig.5

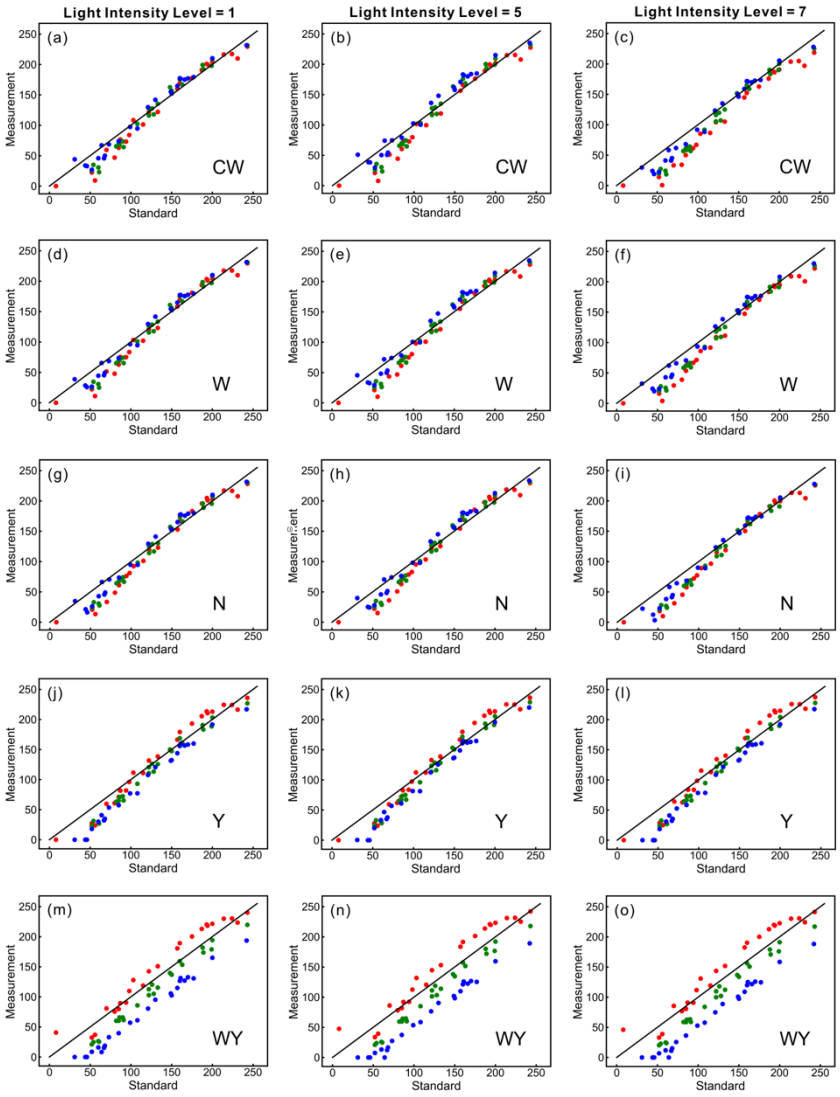
Light Intensity Level = 1
Light Intensity Level = 5
Light Intensity Level = 7
(a)
(b)
(c)
(d)
(e)
(f)
(g)
(h)
(i)
(j)
(k)
(l)
(m)
(n)
(o)
CW
W
N
Y
WY
Measurement
Standard
0
50
100
150
200
250

Fig.6

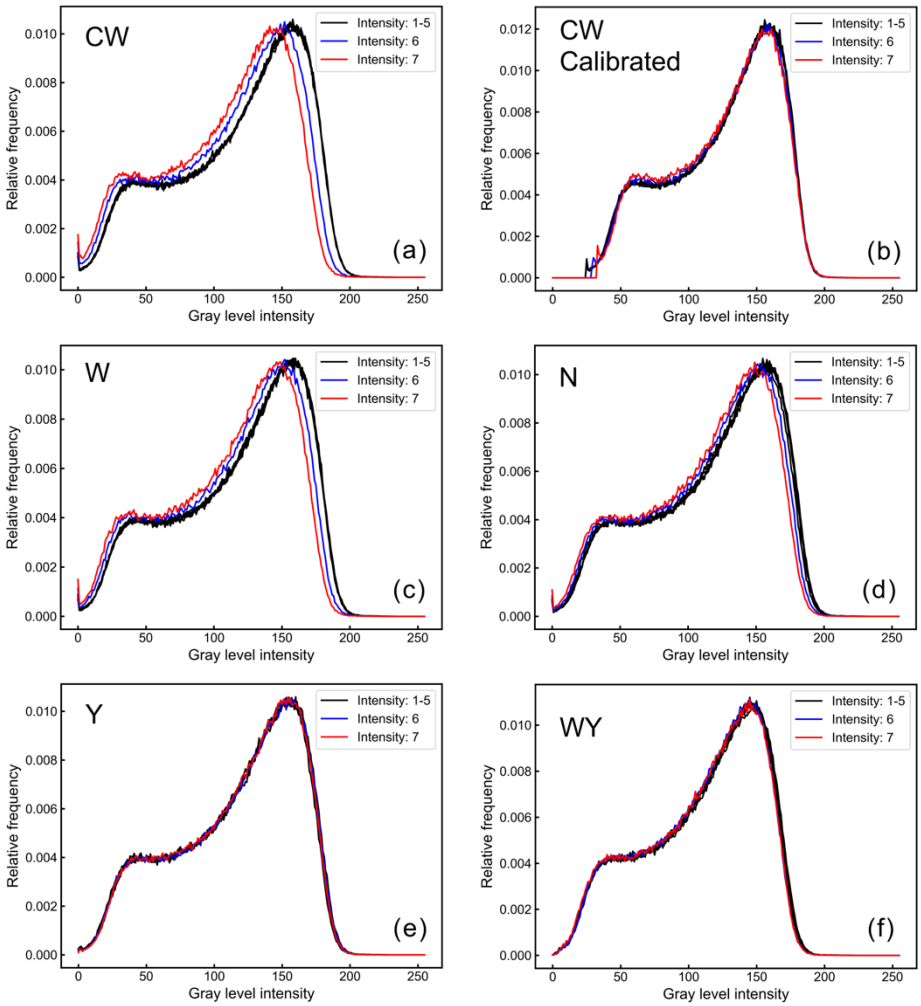
CW
Intensity: 1-5
Intensity: 6
Intensity: 7
(a)
CW
Calibrated
(b)
W
(c)
N
(d)
Y
(e)
WY
(f)
Relative frequency
Gray level intensity

Fig.7

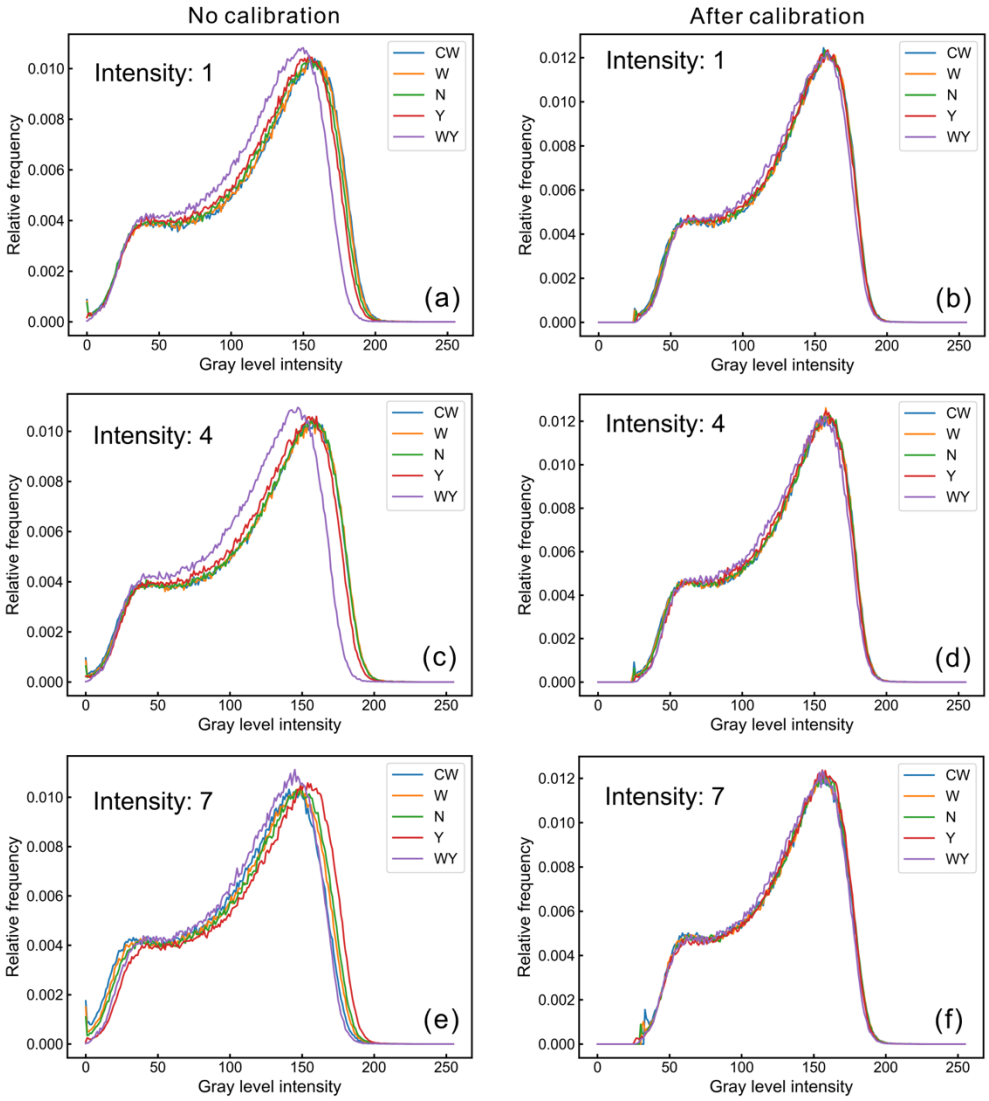
No calibration
After calibration
Intensity: 1
Intensity: 4
Intensity: 7
CW
W
N
Y
WY
Relative frequency
Gray level intensity
(a)
(b)
(c)
(d)
(e)
(f)

Fig.8

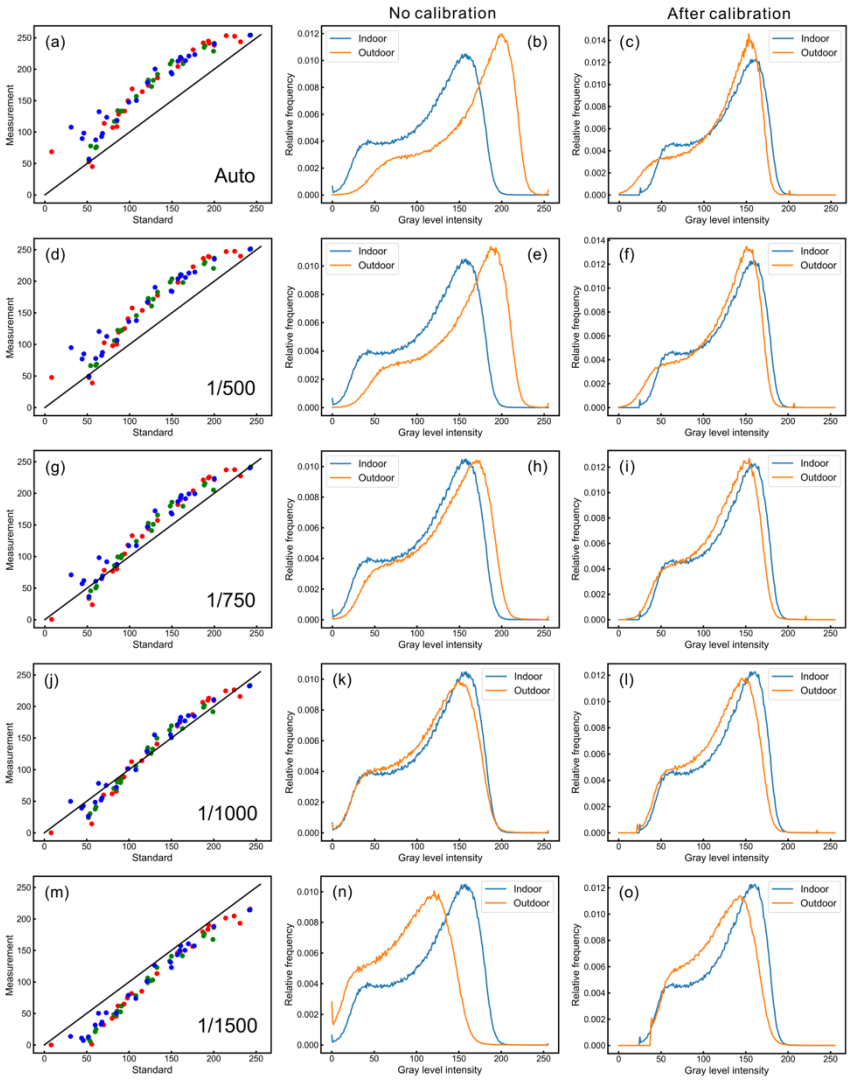
No calibration
After calibration
(a)
Auto
(b)
(c)
(d)
1/500
(e)
(f)
(g)
1/750
(h)
(i)
(j)
1/1000
(k)
(l)
(m)
1/1500
(n)
(o)
Indoor
Outdoor
Measurement
Standard
Relative frequency
Gray level intensity

Fig.9

(a)


MSCCPPCC0817
x-rite
I
II
colorchecker

(b)

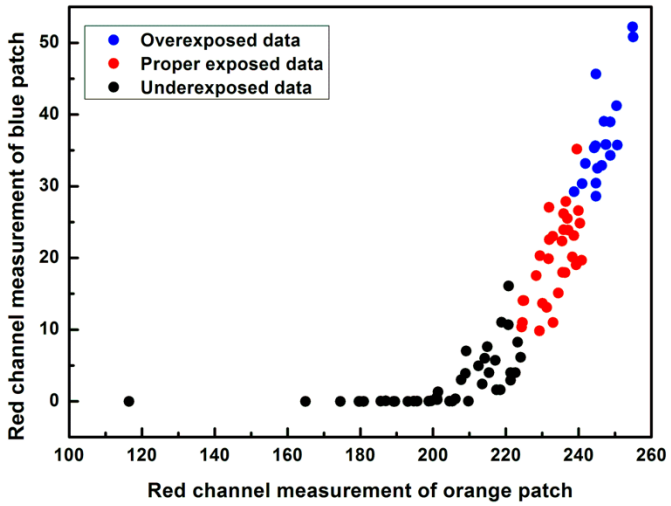
Overexposed data
Proper exposed data
Underexposed data
Red channel measurement of blue patch
Red channel measurement of orange patch
0
10
20
30
40
50
100
120
140
160
180
200
220
240
260

Fig.10

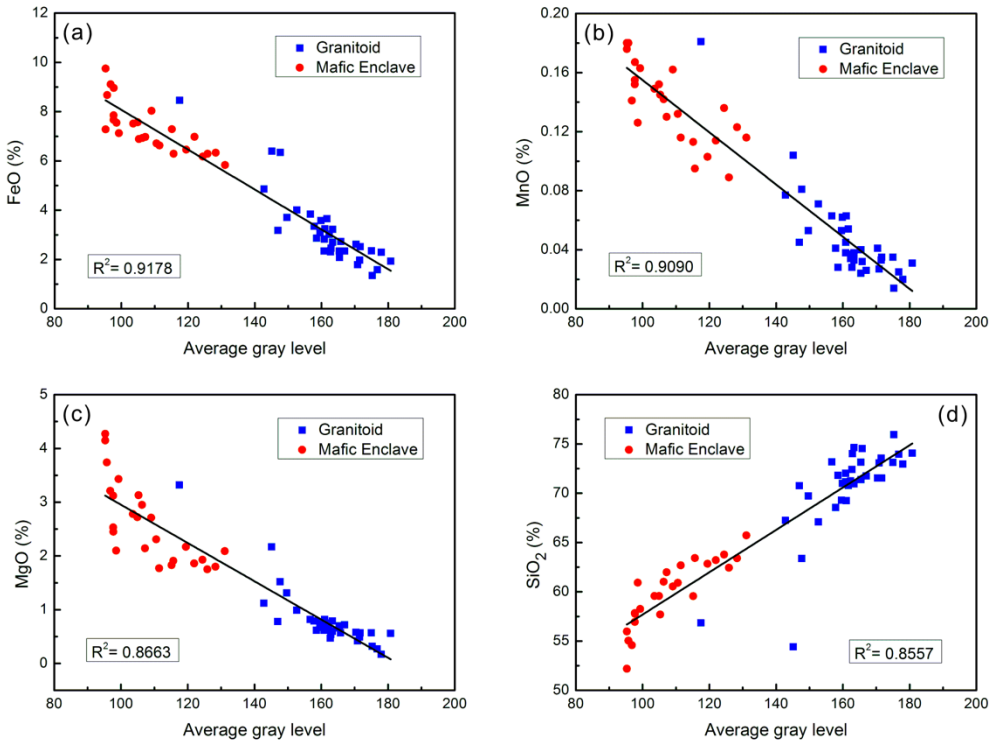
(a)
Granitoid
Mafic Enclave
FeO (%)
R²= 0.9178
Average gray level
(b)
Granitoid
Mafic Enclave
MnO (%)
R²= 0.9090
Average gray level
(c)
Granitoid
Mafic Enclave
MgO (%)
R²= 0.8663
Average gray level
(d)
Granitoid
Mafic Enclave
SiO2 (%)
R²= 0.8557
Average gray level